Published in final edited form as:
Hear Res. 2011 April ; 274(0): . doi:10.1016/j.heares.2010.06.014.

Local connection patterns of parvalbumin-positive inhibitory interneurons in rat primary auditory cortex

Kexin Yuan[a,b], **Kathren L. Fink**[b], **Jeffery A. Winer**[b], and **Christoph E. Schreiner**[a,*]

[a]Coleman Memorial Laboratory and W.M. Keck Foundation Center for Integrative Neuroscience, Department of Otolaryngology, University of California, San Francisco, CA 94143-0444, USA

[b]Department of Molecular and Cell Biology, University of California, Berkeley, CA94720-3200, USA

Abstract

In the auditory cortex (AC), GABAergic neurons constitute approximately 15–25% of all neurons. GABAergic cells are present in all sensory modalities and essential for modulating sensory receptive fields. Parvalbumin (PV) positive cells represent the largest sub-group of the GABAergic population in auditory neocortex. We investigated the projection pattern of PV cells in rat primary auditory cortex (AI) with a retrograde tracer (wheat germ apo-HRP conjugated to gold [WAHG]) and immunocytochemistry for PV. All AC layers except layer I contained cells double-labeled for PV and WAHG. All co-localized PV+ cells were within 2 mm of the injection site, regardless of laminar origin. Most (ca. 90%) of the co-localized PV cells were within 500μm of the injection site in both dorsal-ventral and rostral-caudal dimension of the auditory core region. WAHG-only cells declined less rapidly with distance and were found up to 6 mm from the deposit sites. WAHG-only labeled cells in the medial geniculate body were in ventral division loci compatible with an injection in AI. Differences in the range and direction of the distribution pattern of co-localized PV+ cells and WAHG-only cells in AI express distinct functional convergence patterns for the two cell populations.

Keywords

Auditory cortex; y-Aminobutyric acid (GABA); Parvalbumin; Retrograde tracer; Double-labeling; Local connection

1. Introduction

Gamma-aminobutyric acid (GABA) is the principal inhibitory neurotransmitter of the neocortex (Mugnaini et al., 1985). In primary auditory cortex (AI), GABAergic neurons constitute approximately 15–25% of all neurons (Prieto et al., 1994). This percentage varies among cortical layers from 16% of total neurons in layer VI to 95% in layer I (Prieto et al., 1994). Glutamic acid decarboxylase (GAD), the enzyme responsible for the conversion of glutamate into GABA, also has laminar differences in the number of GABAergic neurons

*Corresponding author. Tel: + 1 415 476 2591; fax: + 1 415 502 4848. kexin@phy.ucsf.edu (K.X. Yuan), thekfink@gmail.com (K.L. Fink), chris@phy.ucsf.edu (C.E. Schreiner).

(Fabri et al., 1996). Classically, GABA is associated with locally projecting inhibitory neurons of the mammalian neocortex via intrinsic horizontal projections (Albus et al., 1994; Albus et al., 1991; Matsubara, 1988) and interlaminar projections (DeFelipe et al., 1985; Somogyi et al., 1981; Somogyi et al., 1983). Recent work on cat (Higo et al., 2007), primate (Tomioka et al., 2007), rat (Fabri et al., 1996) and mouse (Tomioka et al., 2005) also revealed some long distance projections of GABAergic neurons in sensory cortex that may span up to 15 mm.

In auditory cortex, inhibition is thought to play diverse roles in the shaping of neural activity. For example, single unit recordings using two-tone stimuli revealed inhibitory side bands surrounding excitatory receptive filed in cat AI, indicating the operation of 'lateral' inhibitory influences across frequency (Sutter et al., 1999). More recently, *in vivo* whole-cell voltage-clamp recordings showed that, in AC, inhibitory inputs to a neuron are co-tuned to excitatory inputs(Tan et al., 2007; Wehr et al., 2003), allowing for largely balanced excitation and inhibition that determine the temporal precision of spiking outputs of cortical neurons (Wehr et al., 2003). The frequency range of synaptic inhibition and excitation are often only approximately matched, that is, even though the inhibitory cell and its target are preferentially tuned to the same stimuli, inhibitory cells tend to convey a slightly broader synaptic inputs (Wu et al., 2008). This may partly account for the lateral inhibition pattern observed in two-tone stimuli experiments. Broader spectral tuning of putative inhibitory neurons versus pyramidal neurons was also seen in extracellular studies (Atencio and Schreiner, 2008). Studies on synaptic inputs indicated that unbalanced synaptic inhibition can enhance or even create intensity tuned neurons (Greenwood et al., 1965; Phillips et al., 1995; Schreiner et al., 1992), which may play important roles in the encoding of sound level and envelop transients in AC (Tan et al., 2007; Wu et al., 2006). Cortical synaptic inhibition also contributes to the shaping of neural direction selectivity for frequency-modulated sweeps, which is an important temporal cue in animal and human communication (Zhang et al., 2003). All these functional processes require precise coordination between excitatory and inhibitory components. However, the contributions of different types of inhibitory interneurons to auditory cortical receptive fields remain unclear.

GABAergic neurons only represent a small portion of cortical neurons, and they comprise multiple classes of cells distinguished by morphological, connectional, and molecular features (Monyer et al., 2004). The expression of specific calcium-binding proteins in GABAergic neurons, including calbindin (CB), parvalbumin (PV), and calretinin (CR), has been used as one of the criteria to delineate different cell types in neocortex, hippocampus, cerebellum and thalamus (Bastianelli, 2003; Hof et al., 1999; Jinno et al., 2006; Jones, 1998; Markram et al., 2004). Although the specific roles of these proteins in shaping neuronal activity are still debated, it has been proposed that specific types of calcium currents can be selectively modulated by the differential calcium-binding capacity and kinetics observed in these proteins (Schwaller et al., 2002).

Among GABAergic neurons showing calcium-binding protein immunostaining, PV-positive (PV+) cells are particularly interesting since PV is expressed in the largest percent of GABAergic neurons (~40%, Tamamaki et al., 2003) corresponding to ~7% of the total number of neurons in AI (McMullen et al., 1994). Multiple cell morphologies have been observed for cells with immunoreactivity for PV (McMullen et al., 1994; Prieto et al., 1994) including axon-ensheathing chandelier cells and soma-targeting large basket cells. PV+ cells are a major part of the GABAergic population of AI but have exhibited different laminar distributions than the total GABAergic population (McMullen et al., 1994), implying that they represent an anatomically and functionally distinct subpopulation of inhibitory neurons. Developmentally, the onset of the critical period corresponds closely to the emergence of PV+ GABAergic cells (del Rio et al., 1994). Electrophysiological recordings from PV+ cells

have revealed that they are fast-spiking interneurons possibly initiating a feedforward inhibition on their target cells (Mallet et al., 2005). Recent studies using optogenetic manipulation have shown direct evidence that activation of PV+ or fast-spiking inhibitory interneurons can induce gamma oscillations, which are hypothesized to enhance information processing in neocortex (Cardin et al., 2009; Sohal et al., 2009). Detailed spatial quantification of the projection pattern of PV+ cells may further elucidate the function of these cells in auditory cortex circuitry.

Previous studies have quantified the general laminar distribution of cells expressing PV in cat AC (Prieto et al., 1994), but did not determined the specific spatial distribution pattern of PV+ cells projecting to a given locus within AI. This study examines the horizontal, and laminar distributions of PV+ cells that project to an injection site located in AI. Comparing these distribution patterns to the overall GABAergic distribution pattern helps to reveal how PV+ cells may differ in their organization from other inhibitory interneurons in AC. We co-localized PV with wheat germ agglutinin apo-radish peroxidase colloidal gold (WAHG), a retrograde tracer, to reveal the spatial convergence pattern of PV+ and PV− neurons in rat AI. The rat is one of the most widely used animal models for functional studies at the cortical circuit level, especially for *in vivo* whole cell recordings (e.g., Tan et al., 2007; Wehr et al., 2003; Froemke et al., 2007). A more detailed understanding of local inhibitory projection patterns will enhance our ability to disclose and interpret functional processing principles.

2. Methods

2.1 Surgery/Injection

Three male Wistar-Han rats (250–325 grams) approximately 3 months old were used in this study. Buprenorphine (0.05mg/kg s.c.) was administered to each animal before surgery and followed by isoflurane anesthesia. A craniotomy was performed on the left hemisphere above auditory cortex (AC) under aseptic conditions. The retrograde tracer (WAHG) was concentrated by centrifugation and delivered by pressure with a nanoliter injector (W.P.I. Inc., Sarasota, FL) using a glass micropipette with a tip of 30 μm diameter. WAHG was advantageous because it does not interfere with immunocytochemical staining methods (Basbaum et al., 1987) and is not transported in an anterograde manner or taken up by cut or damaged axons (Basbaum, 1989). Three deposits were made in each case at varying cortical depths to label all cortical layers of primary auditory cortex (AI). Deposits were made by five pulses of WAHG at 4.6nl/pulse for a total volume of ~75nl. The location of AI was determined based on landmark features and stereotactic coordinates based on previous physiological studies (unpublished observations). All procedures were conducted in accordance with the University of California, Berkeley Animal Care and Use Committee.

2.2 Tissue Preparation

After a 3–5 day survival time, rats were anesthetized with xylazine (10mg/kg i.p.) and ketamine (90mg/kg i.p.). The deeply anesthetized animals were euthanized with 0.5 ml pentobarbital (50mg/ml i.p.). The thoracic cavity was opened immediately and a canula was inserted through the left ventricle into the aorta. A wash of 0.9% saline with heparin (1ml per 500ml), an anticoagulant, was administered for two minutes and followed by perfusion with Shandon Zinc Formol Fixx (Thermo Fisher Scientific, Waltham, MA) for twenty minutes. After one hour, a post-fix wash of 10% sucrose and 0.9% saline was administered for ten minutes to help cryoprotect the tissue.

The brain was dissected out of cranium, blocked stereotaxically, and cut coronally at the rostral end of cerebellum and rostral end of hypothalamus. Fiducial marks were made in the

right cortex and right hypothalamus of each brain to denote orientation of sections. Each brain was then placed in 30% sucrose, 0.9% saline solution overnight for cryoprotection. The brains were frozen and sectioned (30–40 μm thick) with a microtome and collected in 0.1M phosphate buffer. All cases were sectioned transversely. Sections were collected serially for the entire AC and the ventral division of the medial geniculate nucleus of the thalamus (MGv).

2.3 Immunohistochemistry

Every fourth section was processed for parvalbumin (PV) colocalization in each animal. Sections were incubated in normal horse serum (NHS) followed by 1:5000 primary monoclonal mouse anti-parvalbumin (Swant, Bellinzona, Switzerland) with 2% NHS overnight at 4°C. ABC immunoperoxidase processing (Vector Laboratories, Burlingame, CA) and diaminobenzidine histochemistry revealed PV positive profiles with a dark brown soma and light brown proximal dendrites. Sections were silver intensified (KPL, Gaithersburg, MD) for one hour, rinsed, fixed in sodium thiosulfate, dehydrated, cleared, and coverslipped.

A neighboring section of each parvalbumin-processed section was stained with cresyl violet to reveal presence of Nissl bodies for use in lamina delineation.

2.4 Data Analysis

For each case, the ventral division of the medial geniculate body (MGBv) was analyzed to confirm that the injection was made in AI. Thalamic boundaries were drawn from adjacent Nissl sections without knowledge of labeling (Winer et al., 1999). AI was recognized by its cytoarchitecture (Zilles et al., 1985).

The labeled cells within the auditory cortex were visualized using light microscopy and their locations were plotted and recorded using the Neurolucida image-analysis system (MicroBrightField, Williston, VT). Cells were identified as double-labeled (DL) if PV co-localized with WAHG. Cells labeled with WAHG but not co-localized with PV (single-labeled, SL) were also plotted in sections displaying injection sites in each case. Laminar boundaries were derived from the adjacent Nissl-stained section based on cytoarchitectonic characteristics. Sections were superimposed with aid of advanced graphics software (Canvas, ACD Systems, Victoria, BC) to assess laminar distributions. On sections containing an injection site, AC was divided into 100 μm-wide bins in each layer throughout the injected hemisphere for distance and density calculations in the dorsal-ventral domain. The percentage of DL cells was determined by dividing the number of DL cells by the total number of retrogradely labeled neurons in each bin. Selected sections rostral and caudal to the injection site of case 1846 and 1916 were also plotted to assess the rostral-caudal extent of labeling.

3. Results

In all three cases, the retrograde tracer WAHG was injected into the left hemisphere of AI invading all six cortical layers (Fig. 1A and B). Bright-field microscopy revealed the brown cell profiles that are representative of PV reactivity (Fig. 1A). Dark-field views of these sections identified WAHG labeling as gold granules that outlined WAHG+ only cells. PV+ only cells had brown soma and dendrites and co-localized cells showed brown somas filled with black gold granules (Fig. 1C, D and E, respectively). DL cells represented many morphological types including bipolar and multipolar cells, however no attempt was made to quantify different types. Intensive WAHG labeling was identified in the ventral division of

the medial geniculate nucleus of the thalamus (MGBv) verifying that the deposits significantly involved AI (Fig. 2A and B).

3.1 Dorsal-ventral distribution

In each of the three cases reacted for PV, we quantified the WAHG+ only and DL cells from one section that most ideally displayed the injection site to determine dorsal-ventral cell distribution at its full extent. All measurements are based on plotting WAHG+ only and DL cells (Fig. 3A and B) and by quantifying their distance from the injection site. The distribution was assessed in bins of 100 μm width from the injection site. A total of 345 co-localized cells and 7887 WAHG+ only cells (total = 8232 cells) were identified across these sections from the three animals (mean values per animal: DL: 115 ± 16.6; SL: 2629 ± 921). Adjacent Nissl stained sections were examined to reveal laminar distribution of cells across the six layers of cortex. Cells only labeled for PV were encountered throughout all sections and layers but were not considered further due to their unspecific relationship to the injection site.

Cells with co-localized WAHG and PV+ were found in all layers except layer I. The mean numbers of DL cells per layer in the central section for the three animals were: Layer 1: 0; Layer II: 8±2.6; Layer III: 18±6.9; Layer IV: 17.7±7.4; Layer V: 43±9.8; and Layer VI: 28.3±10.2. The highest number of cells was found in layer V, which was significantly different from all other layers ($p<0.03$; ANOVA with Benferroni correction). Another layer difference was evident between Layer VI and layers II ($p<0.005$). Other layer differences were statistically not significant.

Overall, the number of WAHG+ only cells was about 23 times higher than that of DL cells. The mean numbers of SL cells per layer in the central section for the three animals were: Layer 1: 19.7±24.0; Layer II: 220±161.5; Layer III: 480.3±236.0; Layer IV: 270.3±100.8; Layer V: 755.3±298.0; and Layer VI: 883.3±248.2. The highest number of WAHG-only cells was found in the thicker infragranular layers (Table 1). Both layers were different from layers I, II, and IV ($p<0.01$). Layer VI was also significantly different from layer III ($p<0.03$). The lowest number of WAHG-only cells was seen in layers IV and II.

The highest density of DL versus SL cells was found in layer IV (see Table 1; percentage = DL/(DL+SL)), followed by layer V. This estimate is dominated by the higher cell densities within the first 500 μm from the deposit site (for total cell counts and percentages, see Table 1). Layer IV had a higher DL density than layer II, reflective of potential functional emphasis differences in the various layers.

The density of both WAHG+ only and PV co-localized cells generally decreased with horizontal distance from the edge of the injection track. However, a clear difference in their dorsal-ventral density pattern became apparent. Examples from two cases are shown in Fig. 3A and B. The majority of WAHG-labeled cells (49.3%) were located within 500 μm from the injection site with ~72.1% within 1mm from the deposit (Table 1). The remaining WAHG cells (23.9%) were located more than 1mm distant from the injection site with <5% more than 2mm away. In general, populations of DL cells were also most dense near the deposit, that is, 303 out of 345 DL cells (87.8%) were within 500 μm of the injection site, and 340 DL cells (98.6%) were found <1000 μm from the injection site. However, the density of PV+ cells declined more rapidly with distance than that of WAHG-only cells. The ratio of DL to WAHG-only cells declined from 7.5% within the first 500 μm to 2.0% between 500 to 1000 μm to less than 0.3% beyond 1000 μm, indicating a clear difference in the convergence pattern for inputs from co-localized PV+ and WAHG-only cells.

3.2 Rostral-caudal distribution

The rostral-caudal distribution of SL and DL cells was examined in two cases (Fig. 4A and B). To quantify the rostral-caudal distribution, cells were plotted at a few rostral-caudal distances throughout the coronal sections. Sections analyzed for DL cells were 120 μm apart and assigned to 500 μm distance bins (Table 2). Sections containing the injection site were assigned a distance of zero along the rostral-caudal axis. A total of 1756 DL cells were identified across the two animals.

The number of DL cells decreased with increasing distance from the injection site (Fig. 4A and B). Specifically, out of a total of 1756 co-localized cells, 1599 (91.1%) cells were within 500 μm from the injection site in the rostral- caudal direction and 1754 (99.9%) cells were within 1000 μm (Table 2). This was very similar to the dorsal-ventral distribution with 87.8% and 98.6% for the 500 and 1000 μm distance bins, respectively. Only two cells (0.1%) were located more than 1000 μm away. In the dorsal-ventral direction 1.4% (N=5) of DL cells were found more than 1000 μm from the injection site (Table 1).

Within the range of sections that contained DL cells, only selected sections were plotted and counted for WAHG+ only cells (0, 240, 600, and 960 μm; Table 3) given the large number of labeled cells on each section. Similar to the dorsal-ventral distribution pattern, densest WAHG labeling was found in the sections at 0 and 240 μm from the injection site (Table 3). The percentage of SL cells encountered in the two sections within the first 500 μm (i.e., 0 and 240 μm) was 59.1%, compared to 40.9% in the two sections within 500–1000 μm, (i.e., 600 and 960 μm; Table 3). This decline with distance was shallower than for the 500 and 1000 μm distance bins in the dorsal-ventral direction (68.4 versus 31.6 %). This demonstrates a more rapid decline with distance of DL cells than of WAHG-only cells. In addition the decline of Sl cells was anisotropic with a more rapid decline in the dorsal-ventral direction (30.7%/500 μm) versus the rostral-caudal direction (53.8%/500 μm). DL cells were not observed in layer I along the rostral-caudal axis of both studied cases. Layer II and IV showed the lowest total number (36 and 56, respectively) of DL cells along this direction, however, the relative proportion of DL cells to WAHG-only cells was the highest in layers II and IV (~5%) compared to layers III, V, and VI (~3%) for the 0 and 240 μm sections (Table 3; DL numbers in the other distance bins were too low to calculate meaningful percentages). The furthest projecting DL cells were usually found in layer III and the infragranular layers.

4. Discussion

Few studies have specifically determined the projection pattern of PV+ neurons relative to other cell types in sensory cortex. Most of the studies regarding GABAergic projections assessed the entire GABAergic population using immunoreaction for GABA or glutamic acid decarboxylase (GAD) (e.g., Prieto et al., 1994; McMullen et al., 1994). The few studies specific to PV+ neurons focused on their population size and areal and laminar organization. The function of a neural network is fundamentally determined by interactions between neurons, and the inhibitory population is an essential part of this network. PV+ cells fulfill an important and specific role in the cortical network (Markram et al., 2004). The PV+ population is one of the larger subclasses of the GABAergic cell population, and it is of special interested to determine their projection pattern. In the current study, we demonstrated that in rat AC, first, projections of PV+ cells are local when compared to the distribution of other WAHG-labeled cells, which are predominantly pyramidal cells. Second, local input from PV+ cells generally converged about the same distance in the dorsal-ventral as in the rostral-caudal direction in contrast to the WAHG+ only cells, which show a shallower decline with distance along the rostral-caudal axis. Third, no retrogradely labeled, PV+ cells were present in layer I, and DL cells in layers II and IV had the highest

density when compared to WAHG-labeled cells. These data reveal the projection pattern of PV+ cells from a population point of view, indicating a specific distribution that constrains their potential role in information processing.

In the dorsal-ventral direction, nearly 99% of the co-localized cells examined projected <1,000 μm, and the furthest ones were <1500 μm from the injection site. Several previous studies have observed GABAergic neurons projecting over long distance.Albus et al. (1991) reported that about 30% of retrogradely labeled GABAergic neurons occurred at distances between 1mm and 2.5 mm from the injection site in upper layers of cat striate cortex.Fabri et al. (1996) andHigo et al. (2007) found a subset of GABAergic cells that project well past 1000 μm in rat and cat neocortex, respectively. The study of (Matsubara et al., 1992) showed that in deep layers of cat visual cortex some GABAergic cells spanned greater distances, up to 3.0 mm from the injection center. However, since all of these studies were using immunoreaction for GABA or glutamic acid decarboxylase (GAD), it is not clear if those remote cells were PV+ cells. Tomioka et al. (2005, 2007) also studied long-range GABAergic connections in mouse and monkey neocortex. The vast majority (>90%) of the retrogradely labeled GABAergic neurons remote from their injection sites exhibited somatostatin immunoreactivity and none of them was PV+. Our current study on rat AC further supports this finding and indicates that PV+ neurons may mainly exert their influences locally. It is known that PV+ cells in neocortex show fast-spiking activity (Cardin et al., 2009), which is a functionally important intrinsic property. The fast-spiking behavior and local projection preference of PV neurons likely exerts an influence on target cells that is more efficient and, potentially limited to a narrower range of functional diversity than projections by pyramidal cells.

Of >2000 WAHG-PV co-localized cells, none was found in layer I. However, we did observe a few PV+ only cells in layer I, although their functional influence on the neurons at the injection site is likely weak. This is consistent with the findings byMcMullen et al. (1994) andTamamaki et al. (2003) in rabbit auditory cortex and mouse frontal motor cortex, respectively. Although PV+ GABAergic cells constitute less than 5% of the whole GABAergic population in layer I, the existence of these cells indicates that they must play a functional role in a layer that is dominated by other GABAergic cells. As in previous studies, PV+ cells were most dense in layer IV (e.g., Hendry et al., 1991), however, layer V density was higher than in layer VI in contrast to a cat study by Hendry and Jones (1991). We also observed that most of the remotely located DL cells were in infragranular layers, also a few of those cells were also found in layer II or III (Hendry et al., 1991). Several previous studies (Fabri et al., 1996; Higo et al., 2007; Matsubara et al., 1992; Tamamaki et al., 2003; Tomioka et al., 2007) have shown that, across different cortical areas and species, GABAergic cells in layer V and VI usually span greater projection distances than those in superficial layers.

The spatial range of DL cells in the dorsal-ventral direction was generally the same as in the in rostral-caudal direction. The orientation of the isofrequency domain in rat AI is tilted by about 35° relative to the coronal section plane (e.g., Polley et al., 2007), i.e., the analyzed dorsal-ventral dimension is more closely aligned with the isofrequency domain and the shorter dorsal-ventral axis of AI (~1mm) than with the direction of the frequency gradient and the rostral-caudal axis of rat AI (~3–4mm). The majority of inhibitory, PV+ inputs (90% of DL cells) originate within ±0.5mm of the convergence site. This corresponds to a CF range of ~2 octaves along the tonotopic axis (e.g., Polley et al., 2007; Zhang et al. 2003) compared to ~4 octaves for the pyramidal cell convergence. The convergence distance of PV + cells approximates the full dorsal-ventral extent of rat AI and appears to restrict the majority of PV+ inputs to locations within the field. By contrast, the number of WAHG-only neurons, mostly pyramidal cells, declined much less quickly with distance. In addition,

WAHG-only labeled cells declined even less rapidly along the rostral-caudal direction, roughly corresponding to the tonotopic axis of AI, than in the dorsal-ventral direction, the short, isofrequency axis of AI. This slower decline with distance indicates that those inputs converge from all regions of AI and also from beyond the boundaries of AI. In cat auditory cortex, an anisotropic distribution of local projections has been demonstrated with a tendency that projections along the iso-frequency domain reached farther than along the frequency gradient (Read et al., 2001; Reale et al., 1983). The reason for this discrepancy remains unclear but may be related to the much larger size and modular internal organization of cat AI (Schreiner et al., 2000). DL cells in the dorsal-ventral direction may provide inhibition centered around a similar characteristic frequency, while those in rostral-caudal direction provide inhibitory inputs from adjacent frequency bands. Details of the functional consequences of this type of projection pattern of PV+ cells on AC processing still await clarification.

Supplementary Material

Refer to Web version on PubMed Central for supplementary material.

Acknowledgments

We thank David Larue and Katie Dorsch for technical assistance and Weichen Xu for assistance in data collection and analysis. We also thank Peter Ohara for useful comments on our original manuscript. This work was supported by NIDCD grants R01DC02319 (J.A.W.) and R01DC02260 (C.E.S.).

Jeffs always kind and patient advise, his inspiring mentorship, and his penetrating insights have profoundly influenced all his co-authors and he is deeply missed.

References

Albus K, Wahle P. The topography of tangential inhibitory connections in the postnatally developing and mature striate cortex of the cat. Eur J Neurosci. 1994; 6:779–792. [PubMed: 7521250]

Albus K, Wahle P, Lubke J, Matute C. The contribution of GABA-ergic neurons to horizontal intrinsic connections in upper layers of the cat's striate cortex. Exp Brain Res. 1991; 85:235–239. [PubMed: 1715826]

Basbaum AI. A rapid and simple silver enhancement procedure for ultrastructural localization of the retrograde tracer WGAapoHRP-Au and its use in double-label studies with post-embedding immunocytochemistry. J Histochem Cytochem. 1989; 37:1811–1815. [PubMed: 2479673]

Basbaum AI, Menetrey D. Wheat germ agglutinin-apoHRP gold: a new retrograde tracer for light- and electron-microscopic single- and double-label studies. J Comp Neurol. 1987; 261:306–318. [PubMed: 2442205]

Bastianelli E. Distribution of calcium-binding proteins in the cerebellum. Cerebellum. 2003; 2:242–262. [PubMed: 14964684]

Cardin JA, Carlen M, Meletis K, Knoblich U, Zhang F, Deisseroth K, Tsai LH, Moore CI. Driving fast-spiking cells induces gamma rhythm and controls sensory responses. Nature. 2009; 459:663–667. [PubMed: 19396156]

DeFelipe J, Jones EG. Vertical organization of gamma-aminobutyric acid-accumulating intrinsic neuronal systems in monkey cerebral cortex. J Neurosci. 1985; 5:3246–3260. [PubMed: 4078626]

del Rio JA, de Lecea L, Ferrer I, Soriano E. The development of parvalbumin- immunoreactivity in the neocortex of the mouse. Brain Res Dev Brain Res. 1994; 81:247–259.

Fabri M, Manzoni T. Glutamate decarboxylase immunoreactivity in corticocortical projecting neurons of rat somatic sensory cortex. Neuroscience. 1996; 72:435–448. [PubMed: 8737414]

Greenwood DD, Maruyama N. Excitatory and inhibitory response areas of auditory neurons in the cochlear nucleus. J Neurophysiol. 1965; 28:863–892. [PubMed: 5867883]

Hendry SH, Jones EG. GABA neuronal subpopulations in cat primary auditory cortex: co-localization with calcium binding proteins. Brain Res. 1991; 543:45–55. [PubMed: 2054675]

Higo S, Udaka N, Tamamaki N. Long-range GABAergic projection neurons in the cat neocortex. J Comp Neurol. 2007; 503:421–431. [PubMed: 17503478]

Hof PR, Glezer II, Conde F, Flagg RA, Rubin MB, Nimchinsky EA, Vogt Weisenhorn DM. Cellular distribution of the calcium-binding proteins parvalbumin, calbindin, and calretinin in the neocortex of mammals: phylogenetic and developmental patterns. J Chem Neuroanat. 1999; 16:77–116. [PubMed: 10223310]

Jinno S, Kosaka T. Cellular architecture of the mouse hippocampus: a quantitative aspect of chemically defined GABAergic neurons with stereology. Neurosci Res. 2006; 56:229–245. [PubMed: 16930755]

Jones EG. Viewpoint: the core and matrix of thalamic organization. Neuroscience. 1998; 85:331–345. [PubMed: 9622234]

Mallet N, Le Moine C, Charpier S, Gonon F. Feedforward inhibition of projection neurons by fast-spiking GAB A interneurons in the rat striatum in vivo. J Neurosci. 2005; 25:3857–3869. [PubMed: 15829638]

Markram H, Toledo-Rodriguez M, Wang Y, Gupta A, Silberberg G, Wu C. Interneurons of the neocortical inhibitory system. Nat Rev Neurosci. 2004; 5:793–807. [PubMed: 15378039]

Matsubara JA. Local, horizontal connections within area 18 of the cat. Prog Brain Res. 1988; 75:163–172. [PubMed: 3187050]

Matsubara JA, Boyd JD. Presence of GAB A-immunoreactive neurons within intracortical patches in area 18 of the cat. Brain Res. 1992; 583:161–170. [PubMed: 1380396]

McMullen NT, Smelser CB, de Venecia RK. A quantitative analysis of parvalbumin neurons in rabbit auditory neocortex. J Comp Neurol. 1994; 349:493–511. [PubMed: 7860786]

Monyer H, Markram H. Interneuron Diversity series: Molecular and genetic tools to study GABAergic interneuron diversity and function. Trends Neurosci. 2004; 27:90–97. [PubMed: 15102488]

Mugnaini, E.; Oertel, WH. An atlas of the distribution of GABAergic neurons and terminals in the rat CNS as revealed by GAD immunohistochemistry. In: Bjorklund, A.; Hokfelt, T., editors. Handbook of Chemical Neuroanatomy, Vol. 4, GABA and Neuropeptides in the CNS, Part 11. Elsevier: Amsterdam; 1985. pp. 436408.

Phillips DP, Semple MN, Kitzes LM. Factors shaping the tone level sensitivity of single neurons in posterior field of cat auditory cortex. J Neurophysiol. 1995; 73:674–686. [PubMed: 7760126]

Polley DB, Read HL, Storace DA, Merzenich MM. Multiparametric auditory receptive field organization across five cortical fields in the albino rat. J Neurophysiol. 2007; 97:3621–3638. [PubMed: 17376842]

Prieto JJ, Peterson BA, Winer JA. Morphology and spatial distribution of GABAergic neurons in cat primary auditory cortex (AI). J Comp Neurol. 1994; 344:349–382. [PubMed: 7914896]

Read HL, Winer JA, Schreiner CE. Modular organization of intrinsic connections associated with spectral tuning in cat auditory cortex. Proc Natl Acad Sci U S A. 2001; 98:8042–8047. [PubMed: 11438747]

Reale RA, Brugge JF, Feng JZ. Geometry and orientation of neuronal processes in cat primary auditory cortex (AI) related to characteristic-frequency maps. Proc Natl Acad Sci U S A. 1983; 80:5449–5453. [PubMed: 6193517]

Schreiner CE, Mendelson JR, Sutter ML. Functional topography of cat primary auditory cortex: representation of tone intensity. Exp Brain Res. 1992; 92:105–122. [PubMed: 1486946]

Schreiner CE, Read HL, Sutter ML. Modular organization of frequency integration in primary auditory cortex. Annu Rev Neurosci. 2000; 23:501–529. [PubMed: 10845073]

Schwaller B, Meyer M, Schiffmann S. 'New' functions for 'old' proteins: the role of the calcium-binding proteins calbindin D-28k, calretinin and parvalbumin, in cerebellar physiology. Studies with knockout mice. Cerebellum. 2002; 1:241–258. [PubMed: 12879963]

Sohal VS, Zhang F, Yizhar O, Deisseroth K. Parvalbumin neurons and gamma rhythms enhance cortical circuit performance. Nature. 2009; 459:698–702. [PubMed: 19396159]

Somogyi P, Cowey A, Halasz N, Freund TF. Vertical organization of neurones accumulating 3H-GABA in visual cortex of rhesus monkey. Nature. 1981; 294:761–763. [PubMed: 7322205]

Somogyi P, Cowey A, Kisvarday ZF, Freund TF, Szentagothai J. Retrograde transport of gamma-amino[3H]butyric acid reveals specific interlaminar connections in the striate cortex of monkey. Proc Natl Acad Sci U S A. 1983; 80:2385–2389. [PubMed: 6132386]

Sutter ML, Schreiner CE, McLean M, O'Connor KN, Loftus WC. Organization of inhibitory frequency receptive fields in cat primary auditory cortex. J Neurophysiol. 1999; 82:2358–2371. [PubMed: 10561411]

Tamamaki N, Yanagawa Y, Tomioka R, Miyazaki J, Obata K, Kaneko T. Green fluorescent protein expression and colocalization with calretinin, parvalbumin, and somatostatin in the GAD67-GFP knock-in mouse. J Comp Neurol. 2003; 467:60–79. [PubMed: 14574680]

Tan AY, Atencio CA, Polley DB, Merzenich MM, Schreiner CE. Unbalanced synaptic inhibition can create intensity-tuned auditory cortex neurons. Neuroscience. 2007; 146:449–462. [PubMed: 17320296]

Tomioka R, Rockland KS. Long-distance corticocortical GABAergic neurons in the adult monkey white and gray matter. J Comp Neurol. 2007; 505:526–538. [PubMed: 17924571]

Tomioka R, Okamoto K, Furuta T, Fujiyama F, Iwasato T, Yanagawa Y, Obata K, Kaneko T, Tamamaki N. Demonstration of long-range GABAergic connections distributed throughout the mouse neocortex. Eur J Neurosci. 2005; 21:1587–1600. [PubMed: 15845086]

Wehr M, Zador AM. Balanced inhibition underlies tuning and sharpens spike timing in auditory cortex. Nature. 2003; 426:442–446. [PubMed: 14647382]

Winer JA, Sally SL, Larue DT, Kelly JB. Origins of medial genicul ate body projections to physiologically defined zones of rat primary auditory cortex. Hear Res. 1999; 130:42–61. [PubMed: 10320098]

Wu GK, Li P, Tao HW, Zhang LI. Nonmonotonic synaptic excitation and imbalanced inhibition underlying cortical intensity tuning. Neuron. 2006; 52:705–715. [PubMed: 17114053]

Wu GK, Arbuckle R, Liu BH, Tao HW, Zhang LI. Lateral sharpening of cortical frequency tuning by approximately balanced inhibition. Neuron. 2008; 58:132–143. [PubMed: 18400169]

Zhang LI, Tan AY, Schreiner CE, Merzenich MM. Topography and synaptic shaping of direction selectivity in primary auditory cortex. Nature. 2003; 424:201–205. [PubMed: 12853959]

Zilles K, Schleicher A, Glaser T, Traber J, Rath M. The ontogenetic development of serotonin (5-HT1) receptors in various cortical regions of the rat brain. AnatEmbryol (Berl). 1985; 172:255–264.

ABBREVIATIONS

AC	auditory cortex
AI	primary auditory cortex
APt	anterior pretectum
CB	calbindin
CG	central gray
CP	medial geniculate body, caudal pole
CS	commissure of the superior colliculus
CR	calretinin
D	dorsal nucleus of the medial geniculate body or dorsal
DL	double-labeled
GAD	glutamic acid decarboxylase
GABA	gamma-Aminobutyric acid
M	medial division of the medial geniculate body
MGB	medial geniculate body

MGBd	dorsal division of the medial geniculate body
MGBm	medial division of the medial geniculate body
MGBv	ventral division of the medial geniculate body
PBS	phosphate-buffered saline
PV	parvalbumin
RN	red nucleus
SCi	superior colliculus, intermediate gray
Scp	superior colliculus, deep layer
SCs	superior colliculus, superficial layer
SL	single-labeled
Sl	suprageniculate, lateral par
SNc	substantia nigra, *pars compacta*
SNr	substantia nigra, *pars reticulate*
V	*pars lateralis* of the ventral division *or* ventral
WAHG	wheat germ agglutinin conjugated to apo-horseradish peroxidase

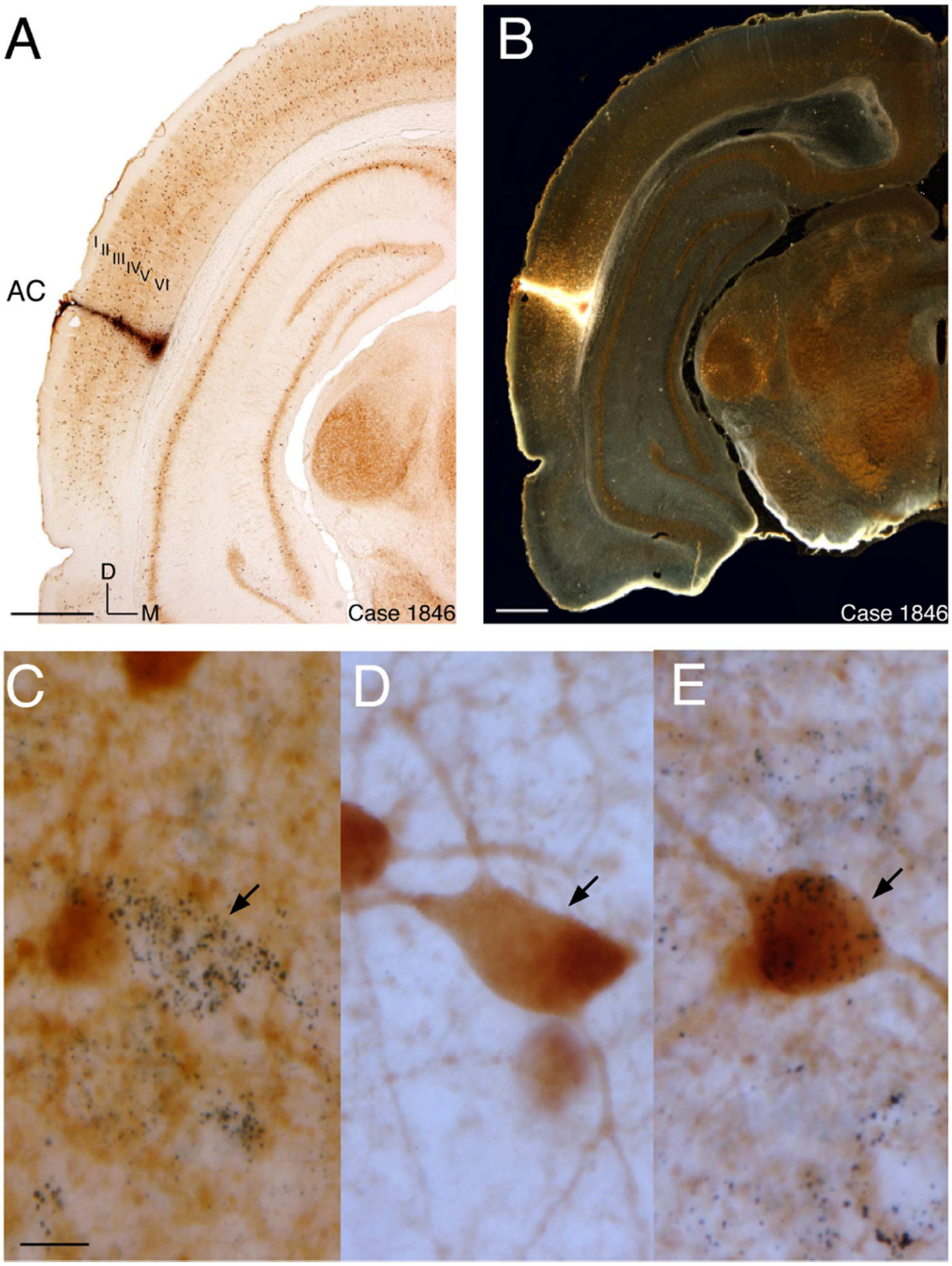

Fig. 1.

(A) Bright-field view of representative tracer (WAHG) deposit in a coronal section. AC: Auditory Cortex; position of cortical layers are indicated by roman numerals from I to VI; Scale bar = 1 mm. (B) Dark-field view of representative tracer deposit in the same coronal section as shown in (A). (C) WAHG+ only cell outlined by black gold granules. Scale bar =15 μm. D and E are of the same scale as C. (D) PV+ only cell with dark brown profile. (E) WAHG and PV co-localized cell.

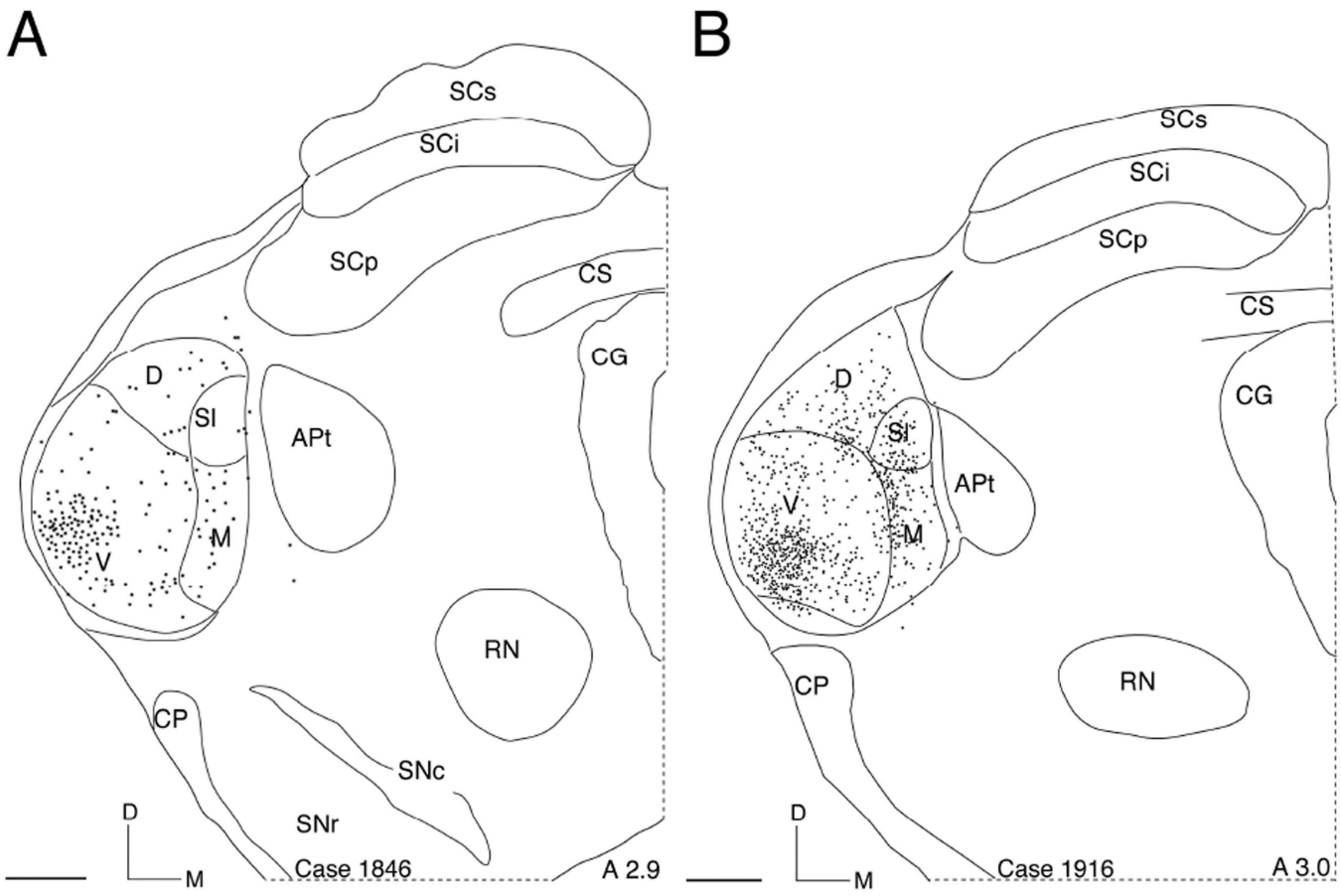

Fig. 2.

(A and B) Neurolucida plots of retrogradely labeled thalamic neurons after injections in AI. A is from the injection shown in Fig. 1. Scale bar = 500 μm. Stereotaxic location relative to the interaural line is indicated.

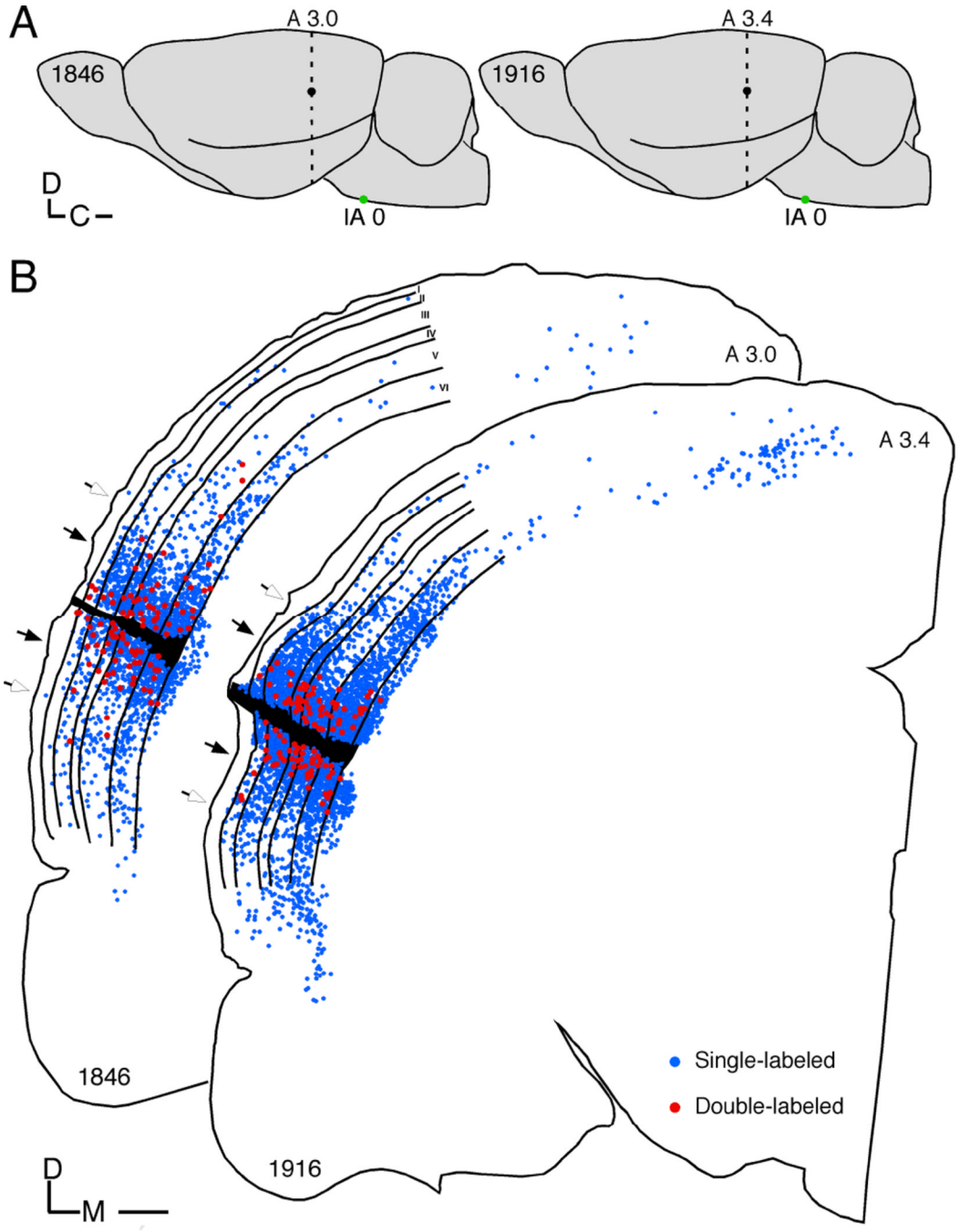

Fig. 3.

(A) Schematic lateral view of rat brain depicting deposit sites (black dot) and position of sections (dashed line) shown in B. Scale bar = 1 mm. Location of interaural (IA) line indicated. (B) Neurolucida plots of the dorsal-ventral and laminar distribution of WAHG+ only (blue dots) and WAHG/PV co-localized (red dots) cells from the two sections depicted in A. Filled and open arrows point to the position of 500 and 1000 μm from the edge of deposit site, respectively. Blue and red dots represent single-labeled and double-labeled cells, respectively. Scale bar = 500 μm.

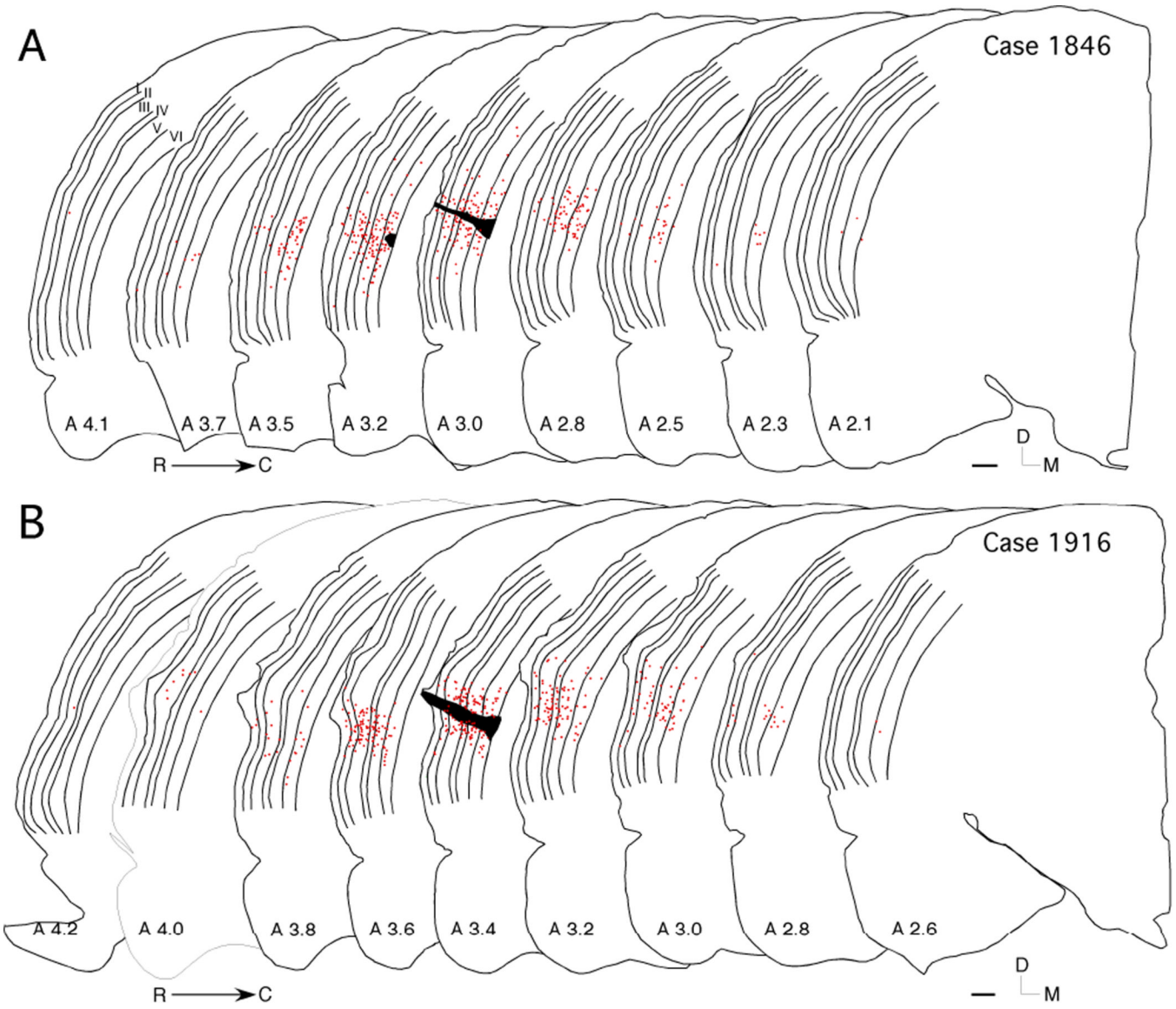

Fig. 4.

(A and B) Rostral-caudal and laminar distribution of WAHG/PV co-localized cells (red dots) for two cases. Injection sites are shown in black; cortical laminae are outlined and labeled (most rostral section). Scale bar = 500 μm.

Table 1

Dorsal-ventral distribution of retrogradely labeled cells on coronal section at the injection site. SL: single-labeled cells, WAHG+ only; DL: double-labeled cells, co-localization of WAHG and PV. Counts are the total of three cases, and are provided for each cortical layer. % = (DLs /Total labeled cells in each bin) * 100.

Three cases	<500 μm			500–1000 μm			>1000 μm			Total		
	DL	SL	%	DL	SL	%	DL	SL	%	DL	SL	%
I	0	33	0	0	13	0	0	13	0	0	59	0
II	20	290	6.5	4	155	2.5	0	215	0	24	660	3.5
III	50	814	5.8	3	404	0.7	1	223	0.4	54	1441	3.6
IV	51	480	9.6	3	175	1.7	0	156	0	54	811	6.2
V	113	1173	8.8	12	521	2.3	4	572	0.7	129	2266	5.4
VI	69	1270	5.2	16	608	2.6	0	772	0	85	2650	3.1
Total	303	4060	6.9	37	1876	1.9	5	1951	0.3	345	7887	4.2

Table 2

Rostral-caudal distribution of DL cells, i.e., co-localization of WAHG and PV. Nine, 8 and 4 sections are included in the three distance bins, respectively; adjacent sections are 120 μm apart. Counts are the total of two cases. % = (DLs in each bin/Total DLs in each corresponding layer) * 100.

Two cases	<500 μm		500–1000 μm		>1000 μm		Total	
	#	%	#	%	#	%	#	%
I	0	0	0	0	0	0	0	0
II	160	89.9	18	10.1	0	0	178	100
III	389	92.6	29	6.9	2	0.5	420	100
IV	189	94.5	11	5.5	0	0	200	100
V	468	94.0	30	6.0	0	0	498	100
VI	393	85.4	67	14.6	0	0	460	100
Total	1599	91.1	155	8.8	2	0.1	1756	100

Table 3

Rostral-caudal distribution of DL and SL cells at four distances from the injection site. Each distance column represents a single section. Counts are the average of two cases. % = (DLs/ Total retrogradely labeled cells in each layer of each section) * 100.

Two cases	0 μm			240 μm			600 μm			960 μm		
	DL	SL	%	DL	SL	%	DL	SL	%	DL	SL	%
I	0	49	0	0	58	0	0	64	0	0	22	0
II	17	286	5.6	14.5	537	2.6	4.5	461.5	1	0	360.5	0
III	40	962	4	44.5	1366.5	3.2	3.5	897	0.4	0.5	640.5	0.08
IV	41	484	7.8	13.5	663.5	2.0	1.5	427.5	0.3	0	319.5	0
V	75	1172	6	59.5	1556.5	3.7	9	994.5	0.9	0.5	763.5	0.07
VI	45	1614	2.7	45	1896	2.3	11.5	1434.5	0.8	1	992.5	0.1
Total	218	4567	26.1	177	6077.5	13.8	30	4279	3.4	2	3098.5	0.25